Coloma, A.; Del Pozo, M.; Martínez-Moro, R.; Blanco, E.; Atienzar Corvillo, PE.; Sánchez, L.; Petit-Domínguez, MD.... (2021). MoS2 quantum dots for on-line fluorescence determination of the food additive allura red. Food Chemistry. 345:1-8. https://doi.org/10.1016/j.foodchem.2020.128628

MoS_2 quantum dots for on-line fluorescence determination of the food additive allura red in beverage

Alicia Coloma[a], María del Pozo[a]*, Rut Martínez-Moro[a], Elias Blanco[a], Pedro Atienzar[b], Lorenzo Sánchez[c], María Dolores Petit-Domínguez[a], Elena Casero[a], Carmen Quintana[a]

[a]*Departamento de Química Analítica y Análisis Instrumental, Universidad Autónoma de Madrid, Cantoblanco, 28049 Madrid, Spain.*

[b]*Instituto Universitario de Tecnología Química CSIC-UPV, Departamento de Química, Universidad Politécnica de Valencia, 46022 Valencia, Spain.*

[c] *Departamento de Medio Ambiente. Geología Ambiental Aplicada. CIEMAT. Avda. Complutense, 40 Edif. 85, 28040 Madrid. Spain*

*maria.delpozo@uam.es; Phone: +34 914975916; Fax: +34914974931

Abstract

This work presents an on-line fluorescence method for the allura red (AR) determination. The method is based on the fluorescence quenching of dots of MoS_2 because of their interaction with the non-fluorescence dye. MoS_2-dots were synthetized and characterized by spectroscopic techniques and High Resolution Transmission Electronic Microscopy (HR-TEM). The simultaneous injection of the nanomaterial and the dye in a flow injection analysis system allows the determination of allura red at 1.7 $\times 10^{-6}$ M concentration level with a very good accuracy and precision (Er minor than 10% and RSD lower than 8%) and a sampling frequency of 180 samples per hour. Moreover, the interaction fluorophore-quencher results a dynamic inhibition mechanism. The proposed methodology was applied to the AR analysis in soft beverages and powders for gelatine preparation. Colourant concentrations of 63±2 mg/L (n=3) and 0.30±0.01 mg/g (n=3) were found, respectively. These results were validated by high performance liquid chromatography technique.

Keywords: Molybdenum disulfide, dots, fluorescence inhibition, allura red, food additive, flow injection analysis.

1. Introduction

Transition metal dichalcogenide (TMDs) nanomaterials are currently attracting the interest of the scientific community because of their promising utilities. TMDs present chemical formula of MX_2, where X belongs to a chalcogenide group, M is a transition metal and both make layers where the metal is located between two layers of chalcogenides, as a sandwich. The adjacent MX_2 layers are bonded through Van der Waals forces, so this weak interaction allows these nanomaterials to be easily exfoliated to thin layers. Therefore, several TMDs nano-morphologies have been reported that can be categorized in different dimensionalities as sheets (2D), nanoribbons and nanotubes (1D) or dots and nanoparticles (0D) (Li et al., 2016). Although many combinations of M and X have been disclosed, molybdenum disulfide and tungsten disulfide are the most frequently employed TMDs. (Bouša et al., 2018; Coleman et al., 2011; S. Xu, Li, & Wu, 2015; X. Zhang et al., 2015)

TMDs nanostructures are produced following bottom-up or top-down approaches.(Sun et al., 2017) Bottom-up syntheses are based on the reaction of metal transition salts with chalcogenide ions, while the stacked structure of bulk TMDs makes them feasible to top-down methods. The most common top-down approach is the ultrasonic-assisted liquid exfoliation in appropriated solvents as N-methyl-pyrrolidone (NMP), dimethylformamide (DMF) or ethanol/water. The advantages of this strategy are such as cheap, easy, scalable and effective, efficiency that is boosted for solvents that minimize the exfoliation enthalpy as NMP. (Huang, Zeng, & Zhang, 2013; Lesnyak, Gaponik, & Eychmu, 2013)

Nanosheets and dots made of TMDs have exhibited their usefulness in the analytical discipline. (Sinha et al., 2018; Vilian et al., 2019) The intrinsic TMDs-dots photoluminescence has encouraged fluorescence methodologies while 2D-TMDs are

more likely to be employed for the development of electrochemical sensors (Vilian et al., 2019). The former approach is based on the ability of some analytes to absorb the photons that dots emit so the output is the dots signal quenching. (Cao et al., 2018; Guo, Wang, Wu, Ni, & Kokot, 2015; X. Liu et al., 2018; Yong Wang & Ni, 2014; Zhao et al., 2017) From this point of view, colourants could be good candidates as analytes in quenching-based methodologies due to their inherent absorption properties.

Colourants are additives in a wide variety of foodstuff giving colour and improving their organoleptic properties. These additives can be classified as natural, semisynthetic and synthetic. Chlorophylls, carotenoids or anthocyanins (natural colourants) are harmless but scarcely resistant to temperature changes, pH or solar radiation (Damodaran, Parkin, & Fennema, 2007). For this reason, synthetic colourants are widely used. This kind of additives are easily synthesized, stables and cheap (Bişgin, 2019). In addition, the sulphonic groups that are present in their chemical structure confer them high solubility in water. The main disadvantage of synthetic colourants is that they usually present azo groups together with aromatic rings in their structures, so they are potentially carcinogens and allergens and can cause hyperactivity in children (Carocho, Barreiro, Morales, & Ferreira, 2014; Ivani de Andrade et al., 2014). Some of these azo-colourants are tartrazine (E-102), sunset yellow (E-110), ponceau 4R (E-124) and allura red (E-129). Its analytical determination has been accomplished by several techniques but especially by high performance liquid chromatography with UV-Vis detector (HPLC-UV-Vis), UV-Vis spectrometry and electrochemical techniques (Bişgin, 2019; Ivani de Andrade et al., 2014; Magerusan et al., 2018). Although colourants are not usually fluorescent, indirect methods based on the interaction with nanomaterials have demonstrated their success (H. Xu, Yang, Li, Zhao, & Liao, 2015).

Flow injection analysis (FIA) is appealing when fast, simple and efficient method is required in routinely performed analysis. These procedures allow automation and miniaturization of analytical methodologies so they have been recognized as very useful in areas such as environmental, industrial and/or clinical analysis. The simple use of its instrumentation makes FIA methods attractive to researchers in the development of analytical methodologies with on-line detection. In addition, a great variety of detectors have been successfully coupled with FIA systems (Trojanowicz & Kołacińska, 2016).

In this work, MoS_2-dots were synthetized and evaluated against the colourant Allura red, employed as food additive. As a result, an on-line FIA method for the determination of this non-fluorescent synthetic dye is developed. The method is based on the fluorescence inhibition of MoS_2-dots due to the interaction with the analyte. The Allura red concentration is monitored thanks to the simultaneous injection of the nanomaterial and the colourant in the flow system. The development of a flow method based on this interaction for the fast and sensitive analysis of non-fluorescent analytes with high sample frequency, results a promising strategy that can be extended to different non-optically active compounds of interest.

2. Materials and Methods

2.1 Reagents

Molybdenum disulfide powder (90 nm, 99%), quinoline yellow, sunset yellow, ponceau 4R, carmoisine, amaranth, sodium citrate, sodium chloride, quinine, glucose, fructose and allura red were obtained from Sigma Aldrich (www.sigmaaldrich.com). N-methylpirrolidone (NMP), orthophosphoric acid, methanol for HPLC, ammonium acetate, acetone and sodium hidroxide were purchased from Scharlab, Spain (www.scharlab.com). Nitric acid for measurements by ICP-MS was tri-distilled

commercial concentrate from Scharlab. Water was purified with a Millipore Milli-Q-System. All solutions were prepared just before use. Inorganic Ventures (Christiansburg, USA) supplied the certified reference molybdenum (995±6 μg/mL) standard for ICP-MS analysis.

2.2 Apparatus

For the MoS_2-dots synthesis, an ultrasound bath (Transonic 570/H Elma) was used. Both, a spectrophotometer Shimadzu UV-1800 and a spectrofluorometer Hitachi F-7000 were employed for optical measurements. A pH meter Methrom C831 (Herisau Switzerland) was used for buffers preparations. The Flow Injection Analysis system employed consisted of i) a peristaltic pump (Heidolph 5201), ii) a 12 ports injection valve (Teknokroma Analítica S.A) equipped with two loops that allows the synchronized injection of nanomaterial and the analyte, converging both at the beginning of iii) the reactor tube producing a homogeneous solution of both reagents and iv) the spectrofluorometric detector operating at fixed excitation and emission wavelengths. A High Performance High Resolution (Element 2) (Thermo Scientific) was employed for Inductively Coupled Plasma - Mass Spectrometry (ICP-MS) measurements. Before the ICP-MS measurements, an acid purification system from Savillex (Eden Prairie, USA) was employed for nitric acid tri-distillation.

High Performance Liquid Chromatography (HPLC) measurements were performed with a Jasco Analytica PU-1580 high pressure pumping system, equipped with an injector Rheodyne Model 7125, a 20 μL loop and a Kromasil C18 column (150 x 4.6 mm; 5 μm; Scharlau). A Perkin Elmer 785A UV/VIS was employed as detector of the chromatographic system.

High Resolution Transmission electron microscopy (HR-TEM) images were acquired with a transmission electron microscope (JEOL JEM 2100F, Tokyo, Japan) under an accelerating voltage of 200 kV. Samples were prepared by applying one drop of the as-synthesised nanodots in NMP onto a carbon-coated copper TEM grid, and allowing it to dry at room temperature. TEM images were analyzed by using Gatan Digital Micrographs software.

2.3 Procedures

2.3.1. MoS_2-dots synthesis

MoS_2-dots were synthesized following a previously reported method (S. Xu, Li, & Wu, 2015) with slight modifications: around 100.00 ± 0.01 mg of the bulk MoS_2 reagent was added to 10.0 mL of NMP and the suspension was exfoliated in an ultrasound bath during 3 h and then heated at 140 °C under stirring during 6 h. After leaving to rest overnight, the mixture was centrifuged at 4000 rpm for 45 minutes. MoS_2-dots were separated in the supernatant and kept at 4 °C until use. From the ICP-MS analysis of the as-prepared nanomaterials, it was found a synthesis yield of 2.02%.

2.3.2. Spectroscopic measurements

Absorbance spectra were acquired between 250 and 800 nm with a 1 cm quartz cuvette. For spectrofluorometric measurements, an excitation wavelength (λ_{ex}) of 370 nm was employed with a slit of 5.0 nm and the fluorescence was recorded from 380 to 600 nm with 1 cm path length when static measurements were performed.

The MoS_2-dots concentration was quantified by ICP-MS. To this end, after the solvent evaporation, the MoS_2-dots were dissolved in a 1:1 (v/v) HNO_3:HCl mixture, as previously described in the literature (W. Zhang et al., 2015). After an adequate dilution, the samples were subjected to ICP-MS determination. The Mo quantification

was performed at low resolution (LR) at m / ΔM = 300. The tune parameters employed were: plasma power = 1258 Watt, pump speed=15 rpm, cool gas = 16 L/min, auxiliary gas =1.3 L/min, sample gas = 1.2 L/min, extraction voltage = -2000 V, SEM = 1900 V. Mass spectrometric data were acquired in EScan mode at the following conditions: segment duration = 0.15 s, settling time = 0.001 s, sample time = 0.015 s, samples per peak = 50, acquired points = 10, detection mode = analogical + counting, integration window = 20%. The isotope ^{95}Mo was monitored, in a mass range of 94.874 - 94.937 u and with the same mass window of 20%. Sample introduction was performed with a peltier cooled inlet system with quartz cyclonic spray chamber (ESI: Elemental Scientific Instruments, Omaha EEUU).

FIA measurements were carried out with fluorescence detection at λ_{exc} = 370 nm and an emission wavelength (λ_{em}) of 475 nm. H_3PO_4/NaH_2PO_4 0.1M buffer pH =2 was employed as carrier solution pumped at a constant flow rate of 3 mL/min. A volume of 100 µL of MoS_2-dots (150 fold diluted in water) and 100 µL of analyte were synchronously injected in the flow system and the successive reaction was produced in a 40 cm reactor with an internal diameter of 0.5 mm.

HPLC-UV measurements were performed following a previously reported procedure (Yu & Fan, 2016) with a flow rate of 0.7 mL/min.

2.3.3. Sample preparation

Two commercially samples were acquired in a local market, a carbonated drink and a powder for gelatine preparation. The soft drink of strawberry flavour was degassed under stirring and, after 10 times dilution with carrier solution, was injected in the FIA system. For HPLC-UV analysis, the carbonate drink samples were degassed as described above and diluted (1:10) with Methanol/ammonium acetate 0.02 M (35/65,

v/v) employed as mobile phase. Next, the diluted samples were filtered through a 0.45 μm pore size nylon filter before injection in the chromatographic system.

An accurate amount of gelatine sample of around 3.00000 ± 0.00001 g was crushed with a mortar. The sample was successively extracted first with methanol and then with acetone by tip sonication according to a published procedure (Shen, Zhang, Prinyawiwatkul, & Xu, 2014). After centrifugation at 4000 rpm for 5 minutes, the extracts were mixed up and evaporated under nitrogen stream until nearly dryness. The residue was reconstituted in methanol and filled up to 5.00 mL. Before to be injected in the FIA system, 150 μL of the extract were diluted to 1.00 mL in the carrier solution. For HPLC analysis, 15 μL of the sample extract were diluted with mobile phase to 5.00 mL before filtration and injection.

3. Results and discussion

3.1 Nanomaterials characterization

3.1.1. High-Resolution Transmission Electron Microscopy experiments

The synthesized dots of MoS_2 were characterized by HR-TEM to obtain information related to its particle size and crystallinity. Figure 1A shows an example of the HR-TEM images obtained where individual and very small nanoparticles of around 5 nm or minor, are observed. Moreover, in the marked zone of the image, the lattice fringes revealing the nanoparticles crystallinity can be clearly observed, also Fast Fourier Transform (FFT) analysis support this observation. From the data of N = 90 nanoparticles, a mean diameter of (3.4 ± 0.9) nm was calculated. The electron diffraction (SAED) pattern of the inset in Figure 1A reveals the hexagonal lattice

structure with a lattice parameter of 0.27 nm (calculated from inverse FFT image after selecting the diffraction spots) and similar with the direct measurement of profile plot (Figure 1B and 1C), consistent with the (100) diffraction planes of MoS_2 (Ha, Han, Choi, Park, & Seo, 2014; Q. Liu, Hu, & Wang, 2016; Yichao Wang et al., 2013).

FIGURE 1 HERE.

3.1.2. Spectroscopic characterization

First, the MoS_2-dots concentration was evaluated by the ICP-MS procedure described above. Figure S1 depicts the calibration graphs corresponding to the Mo determination. From this analysis, the concentration MoS_2-dots was 0.202 mg/mL.

Next, the MoS_2-dots synthesized in NMP were subjected to spectroscopic characterization after a 1:100 dilution in water. The MoS_2-dots UV-Vis spectrum (Figure S2A) displays two absorption bands centred at 270 and 340 nm. These two bands are the maxima characteristic of TMDs-dots and are ascribed to the electronic transitions of π to π^* and n to π^*, respectively (X. Liu et al., 2018). Notice that no features were recorded at longer wavelengths. Unlike TMDs-dots, TMDs-nanosheets show up to four absorption bands in the 390-680 nm domains so the effective transformation of nanolayers into dots can be concluded (X. Liu et al., 2018; Wilcoxon, Newcomer, & Samara, 1997; H. Xu et al., 2015; S. Xu et al., 2015a). Moreover, as stated in the introduction section, TMDs-dots have inherent photoluminescence (Štengl & Henych, 2013). For this reason, it was recorded the emission spectra at different excitation wavelengths around both UV-Vis maximums. The spectra in Figure S2B confirm that: i) a luminescent nanomaterial was synthetized as expected; ii) irrespective of the excitation wavelength (λ_{exc}) used, MoS_2-dots present an emission band with a

maximum at 458 nm (λ_{em}); iii) the fluorescence intensity depends on $\lambda_{exc,}$ recording the highest intensities when exciting at λ_{exc} 270 and 370 nm.

The influence of the pH of the solution on the MoS_2-dots fluorescence was tested by varying the pH solution in which the dots suspension was diluted. Figure S3 depicts the results corresponding to MoS_2-dots excitation at 370 nm. As observed, the fluorescence intensity decreases as pH increases, recording the maximum fluorescence value at acidic media. Moreover, the fluorescence signal is not affected by the presence of salts in solution as can be concluded by comparing the spectra recorded in un-buffered water and neutral pH phosphate buffer. It should be noted the large decrease in the signal showed at alkaline conditions. This pH dependence was also observed when 270 nm λ_{exc} was used (data not shown). As the highest intensity signal is obtained with 0.1 M H_3PO_4/NaH_2PO_4 pH 2, this pH was selected as the measurement medium for the rest of experiments.

In this pH 2 medium, we calculated the relative fluorescence quantum yield of the MoS_2-dots, employing quinine as standard (Φ tabulated $\lambda_{exc\ 275\ nm}$ = 0.577) and according to equation 1 below:

$$\Phi_x = \Phi_s \frac{A_s}{A_x} \cdot \frac{F_x}{F_s} \cdot \left(\frac{n_x}{n_s}\right)^2$$

Equation 1. Φ = fluorescence quantum yield, A = absorbance at λ_{exc}, F = emission curve area, n = solvent refraction index. Subscripts *s* and *x* correspond to the standard and the analyte respectively.

From the results, a value of 8.6% was obtained which is similar or better that other values previously reported in the literature for MoS_2-dots and carbon dots (Cao et al., 2018; Yong Wang & Ni, 2014; Z. Wang & Dai, 2015).

249

250 3.2 MoS_2-dots interaction with Allura red. Static conditions.

251 The absorbance spectrum of a 2.0×10^{-5} M AR solution shows two absorption bands
252 between 300 and 600 nm (Figure 2A, curve a). However, it is important to note that no
253 fluorescence is registered for this dye neither when exciting at its maximum absorption
254 wavelength (500 nm) or exciting at the MoS_2-dots excitation wavelength (270 and 370
255 nm) (data not shown). In addition, Figure 2A includes the fluorescence spectra of MoS_2-
256 dots (dotted lines). As can be seen, these emission spectra overlap in a great extent with
257 the absorption spectrum of the colourant. This result led us to expect an interaction
258 between the nanomaterial and the AR based on the energy/photon transfer of MoS_2-dots
259 emission to the colourant.

260 FIGURE 2 HERE

261 To verify the interaction of the nanomaterial with AR, the fluorescence spectra of a
262 solution containing a mixture of both, MoS_2-dots and AR, were registered either at λ_{exc}=
263 270 nm or λ_{exc} = 370 nm. Figure 2B shows the fluorescence response of the dots and the
264 dots in presence of 2.0×10^{-5} M of AR at λ_{exc} = 370 nm. As observed, the nanomaterial
265 fluorescence is greatly quenched in presence of AR probably because of the analyte
266 absorbs the nanomaterial emission leading to a fluorescence reduction in a dynamic
267 mechanism as will be latter discussed. The same behaviour is observed when excitation
268 is performed at 270 nm (data not shown). We selected 370 nm as excitation wavelength
269 since better selectivity is expected than working at lower excitation conditions.

270 Once the nanomaterial-AR interaction was experimentally confirmed, a deeper study of
271 this interaction was carried out. The Stern-Volmer constant (K_{sv}) determines the degree

of interaction fluorophore - quencher (Lakowicz, 2006) and it is calculated from the same name equation:

$$\frac{If_0}{If} = 1 + K_{sv}[Q]$$

Equation 2. Stern-Volmer equation.

In this equation, If_0 and If correspond to the MoS_2-dots emission in absence and in presence of a concentration of colourant, [Q]. The meaning of the calculated constant is that the higher the K_{sv} value, the stronger the interaction. For K_{sv} determination, the MoS_2-dots spectrum was registered in presence of increasing concentrations of AR. Figure 3 shows the obtained results of If_0/If versus AR concentration. The monitoring of the dots emission was performed at λ_{em} of 475 nm where the quenching due to the interaction with AR is more remarkably produced (see Figure 2B). This experiment was performed at different temperature values.

FIGURE 3 HERE

As shown in Figure 3, linear relations between If_0/If and AR concentration are obtained in all experiments. From the corresponding slopes, the K_{sv} values can be calculated (see the legend Figure 3). Data shows a slight increase in K_{sv} with the temperature. This increase would imply a dynamic inhibition mechanism in which diffusion could control the interaction. This diffusion is favoured by increasing the temperature, making greater the constant value (X. Liu et al., 2018).

Finally, the influence of the concentration of MoS_2-dots was studied to obtain the best analytical response in terms of sensitivity. To this aim, several nanomaterial dilutions (1:50-1:200) in 0.1 M H_3PO_4/NaH_2PO_4 pH 2 were prepared and assayed against two analyte concentration levels, [AR] = 1.25×10^{-6} M and [AR] =2.00×10^{-5} M (data not

shown). From the results, the best accomplishment was obtained for a 150-fold dilution. Therefore, this condition was selected for the development of the FIA analytical method towards the on-line AR determination.

3.3 MoS_2-dots interaction with AR in flow conditions. FIA experiments.

FIA measurements were carried out with fluorescence detection at λ_{exc} = 370 nm and an emission wavelength (λ_{em}) of 475 nm. Figure S4 shows that the synchronized injection of MoS_2-dots and AR produces a decrease in the height peak confirming the interaction MoS_2-dots-AR in the carrier flow towards the fluorescence detection system. This simple experiment allows us to conclude that the quenching effect can be monitored also under flow conditions. Therefore, the optimization of the experimental variables affecting to the FIA system was following made.

3.3.1. FIA optimization: hydrodynamic and geometric parameters.

The hydrodynamic and geometric parameters involved in the FIA response were optimized in order to obtain the highest fluorescence quenching (% $If_0 = \frac{If}{If0} \cdot 100$) as well as the highest sample frequency. Caudal (Q), reactor length (L), reactor internal diameter (Di) and injection volume (Vinj) were optimized. First, the influence of the carrier flow rate was evaluated in the 1 to 4 mL/min range. The results did not show a noticeable influence in the $\%If_0$ but the sample frequency increases while increasing the caudal, because of the decrease of the peak width (Figure S5). This effect is produced up to a flow rate value of 3 mL/min, when the signal is stabilized. Therefore, this flow rate was considered as optimal for the rest of experiments.

Six reactors were used to optimize length (L = 40, 70 and 100 cm) and internal diameter (Di = 0.5 and 0.8 mm). As seen in Figure S6, the thinnest internal diameter reactor showed better $\%If_0$ regardless of the length. For each Di value, a shortened reactor showed a slightly better $\%If_0$. In base of these results, a reactor with Di = 0.5 mm and L = 40 cm was selected for the analytical determination.

Sample loops were simultaneously varied between 50 and 200 µL volume keeping the same volume for the analyte and the MoS_2-dots. As in previous experiments, $\%If_0$ was scarcely affected. However, it was found that the higher the loop volume, the wider the FIA signal peaks so poorer sampling frequencies were registered. From the results (Figure S7), 100 µL volume was fixed for further assays. Altogether, the optimal parameters summarized in Table S1 allow the analysis of 180 samples/h in conjunction with a good fluorescence inhibition.

3.3.2. Influence of AR concentration in the analytical response. Analytical data

Once all the variables affecting the FIA system were optimized, the quenching in the fluorescence intensity of MoS_2-dots with increasing AR concentrations was studied. Figure 4 shows that a linear decrease of the initial signal was obtained in the AR concentrations range of 5.00×10^{-6} M to 4.00×10^{-5} M according to the equation: $\%If_0 = -1.2 (\pm 0.3) \times 10^6$ [AR] (M) + 99.0 (± 0.6); r=0.995.

FIGURE 4 HERE

Detection limit (LOD) and determination limit (LOQ) for the analytical method were calculated from the standard deviation (σ) of 10 injections of MoS_2-dots in the FIA system and the slope of the corresponding linear range of the calibration curve. The obtained values were 1.7×10^{-6} M and 5.6×10^{-6} M for LOD (3σ/slope) and LOQ (10σ/slope), respectively. These results are comparable with those reported in the

341 literature for the AR determination with different analytical methodologies (see Table
342 S2) (Al Shamari et al., 2020; Deroco, Medeiros, Rocha-filho, & Fatibello-filho, 2018;
343 Mazdeh et al., 2016; Rodriguez, Ibarra, Miranda, Barrado, & Santos, 2016; Silva,
344 Garcia, Lima, & Barrado, 2007; Tang et al., 2018; Vidal, Garcia-Arrona, Bordagaray,
345 Ostra, & Albizu, 2018). Compared with the analytical methods summarized in Table S2,
346 the proposed method presents several advantages such as allowing a fast analysis with a
347 high sample frequency and the possibility of an on-line analysis automation.

348 Table 1 summarizes the results obtained to evaluate the accuracy and the precision in
349 terms of the relative error (Er %) and the relative standard deviation (RSD %). The
350 precision was assessed in both, repeatability and reproducibility for five concentrations
351 levels. As seen, the developed method presents Er (%) values lower than 10% and
352 excellent results in terms of repeatability and reproducibility with RSD (%) values
353 lower than 1.3% and 8%, respectively.

354

355 **Table 1.** Er (%) and RSD (%) for the developed method at different AR concentrations.

[AR] (M)	**Er (%)**	**RSD (%) $_{(n = 3)}$ repeatibility**	**RSD (%) $_{(n = 3)}$ reproducibility**
1.25×10^{-5}	4.0	0.6	3
1.50×10^{-5}	6.7	0.7	4
2.00×10^{-5}	10	0.3	6
3.00×10^{-5}	3.3	1.2	8
4.00×10^{-5}	5.5	1.3	7

356

357 *3.3.3. Interference study*

358 The selectivity of the method was evaluated by the change that it is produced in the
359 fluorescence signal of a mixture of MoS_2-dots with 2.00×10^{-5} M of AR in presence of
360 increasing amounts of different compounds that can be present in a sample together

with the analyte. It was considered that interference is produced at a concentration level that led to a change in the initial analytical signal bigger than the relative error of the method (10%). Sodium citrate, sodium chloride, glucose and fructose were selected because they are usually found in carbonated drinks. Both salts can be present in high concentration respect to AR, even to 200-fold, without produce interference. Concerning glucose and fructose, the obtained results show that the maximum concentrations allowed without producing interference are 0.37 M and 0.055 M, respectively. These results show the possibility to determine AR in presence of high concentration of sugar. The rest of compounds assayed were other colourants that can also appear with the analyte in some samples. Amaranth, quinoline yellow, ponceau 4R, carmoisine and sunset yellow interfere for a concentration higher than 2.80×10^{-5} M, 2.03×10^{-5} M, 8.03×10^{-6} M, 1.50×10^{-5} M and 2.00×10^{-5} M, respectively. These results show that it is possible to determine AR in presence of other colourants.

3.3.4. Application to AR determination in real samples.

The feasibility of the method was tested towards the AR determination in real samples of a commercial carbonated drink of strawberry flavour and a powder to prepare gelatine. The procedures for each sample preparation were previously detailed in the experimental section. In the case of the carbonated drink, only a degas pre-treatment of the beverage was needed. The determination was carried out by the injection in the FIA system of non-spiked samples and samples spiked with increasing AR concentrations. The FIAgrams in Figure 5 show the decrease produced in the MoS_2-dots fluorescence intensity when the non-spiked sample was injected. This fact allows us to conclude the presence of AR in the selected sample, as it was described in the available information of the drink. As expected, the fluorescence quenching linearly increases with increasing

amounts of AR added according to the equation: $\%If_0 = (-1.2 \pm 0.6) \times 10^6$ [AR] (M) + (82.5 ± 0.7); r = 0.994. As observed, the slope obtained with the standard addition method is the same than that gotten with the external calibration procedure described before. This fact suggests that no matrix interference was produced. Therefore, the external calibration was employed to determine the AR concentration in the sample obtaining a value of 63±2 mg/L (n= 3) of AR in the beverage. Due to the legal limit established by the Council of the European Union of AR in this kind of samples is 100 mg/L, this sample is appropriate for human consumption (Union, 1994). The recovery of the method was evaluated from the analysis of an initially spiked sample at 2.00×10^{-5} M AR concentration. A recovery of 105% with a RSD of 3.8% as average of three independent analyses was calculated.

For the AR determination in gelatine samples, aliquots of 150 µL of non-spiked and spiked with increasing AR amounts sample extracts (obtained as described in section 2.3.3.) were diluted to 1.00 mL and injected in the FIA system. In this case, a linear decrease of the % If with the increase of AR fitted with the equation: $\%If = 85.4 \pm 0.3 - (6.03 \pm 0.09) \times 10^5$ [AR] (M). The difference in the slope observed with respect to that obtained with the calibration graph ($-1.2 (\pm 0.3) \times 10^6$ M^{-1}), shows the influence of these matrix in the AR determination. Therefore, the colourant concentration was calculated from the addition standard procedure. An AR amount of 0.30 ± 0.01 mg/g (n=3) was obtained in this sample with a recovery of 96%, evaluated at 2.00×10^{-5} M concentration level.

FIGURE 5 HERE

3.3.5. HPLC-UV-Vis experiments

In order to validate the result obtained by the FIA-based methodology, both the carbonated drink and the powder for preparation of gelatines were further analysed by HPLC-UV-Vis detection following a procedure previously reported (Yu & Fan, 2016). Figure S8 shows the chromatographs corresponding to increasing AR concentrations. As observed, AR was detected at a retention time (t_R) of 7.6 min and the increase of the signal with AR concentration. Under these conditions, the area values recorded for the injection of the samples, prepared as described before, were $(2.18 \pm 0.01) \times 10^5$ for the carbonated drink and $(1.65 \pm 0.03) \times 10^4$ in the case of the gelatine sample. From the slope of the calibration curve $(1.76 \pm 0.8) \times 10^{10}$ Area/ M), AR concentrations of 61.4 ± 0.3 mg/L (n=3) and 0.297 ± 0.006 mg/g (n=3) were respectively obtained. These results are in very good agreement with that found with the FIA method proposed allowing us to confirm that the herein reported method works for routine determination of this food additive in real samples.

4. Conclusions

In this work, we have demonstrated that dots of MoS_2 results an interesting nanomaterial for the analytical method development based on its fluorescence properties. The HR-TEM reveals very small nanoparticles of 3.4 nm with a hexagonal lattice structure consistent with the (100) diffraction planes. This nanomaterial presents a fluorescence response with a maximum centred at 458 nm when excited with an excitation wavelength of 370 nm. The inhibition of the MoS_2-dots fluorescence signal is

produced due to the interaction with the dye AR as analyte. The simultaneous injection of the nanomaterial and the analyte in the flow system allows monitoring of the AR concentration. After parameters optimization, the obtained results reveal a sensitive method with a LOD of 1.7 x 10^{-6} M and a sample frequency of 180 samples/h. This method was applied in the AR determination in a carbonated commercial drink and powder for gelatine with a recovery of 105 % and 96%, respectively. These results were in good agreement with the obtained with a HPLC-UV-Vis method.

5. Acknowledgements

The authors acknowledge financial support from the Spanish MICINN (MAT2017-85089-C2-2-R), the Comunidad Autónoma de Madrid (P2018/NMT-4349, TRANSNANOAVANSENS-CM).

6. References

Al Shamari, Y. M. G., Alwarthan, A. A., Wabaidur, S. M., Khan, M. A., Alqadami, A. A., & Siddiqui, M. R. (2020). New Ultra Performance liquid chromatography-mass spectrometric method for the determination of allura red in soft drinks using corncob as solid phase extraction sorbent: Analysis and food waste management approach. *Journal of King Saud University - Science*, *32*(1), 1135–1141. https://doi.org/10.1016/j.jksus.2019.10.011

Bişgin, A. T. (2019). Simultaneous Extraction and Determination of Allura Red (E129) and Brilliant Blue FCF (E133) in Foodstuffs by Column Solid-Phase Spectrophotometry. *Journal of AOAC International*, *102*, 181–188.

Bouša, D., Mayorga-Martinez, C. C., Mazánek, V., Sofer, Z., Boušová, K., & Pumera, M. (2018). MoS2 Nanoparticles as Electrocatalytic Labels in Magneto-

Immunoassays. *ACS Applied Materials and Interfaces*, *10*(19), 16861–16866. https://doi.org/10.1021/acsami.8b01607

Cao, H., Huang, Y., Xie, Y., Shi, W., Fu, C., & He, W. (2018). A fast-responsive fluorescent probe for sensitive detection of graphene oxide based on MoS_2 quantum dots. *The Analyst*, *143*(13), 3107–3113. https://doi.org/10.1039/C8AN00849C

Carocho, M., Barreiro, M. F., Morales, P., & Ferreira, I. C. F. R. (2014). Adding Molecules to Food , Pros and Cons : A Review on Synthetic and Natural Food Additives. *Comprehensive Reviews in Food Science and Food Safety*, *13*, 377–399. https://doi.org/10.1111/1541-4337.12065

Coleman, J. N., Lotya, M., O'Neill, A., Bergin, S. D., King, P. J., Khan, U., Young, K., Gaucher, A., De, S., Smith, R. J., Shvets, I. V., Arora, S. K., Stanton, G., Kim, H-Y., Lee, K., Kim, G. T., Duesberg, G. S., Hallam, T., Boland, J. J., Wang, J. J., Donegan, J. F., Grunlan, J. C., Moriarty, G., Shmeliov, A., Nicholls, R. J., Perkins, J. M., Grieveson, E. M., Theuwissen, K., McComb, D. W., Nellist, P. D., Nicolosi, V. (2011). Two-Dimensional Nanosheets Produced by Liquid Exfoliation of Layered Materials. *Science*, *331*(6017), 568–571. https://doi.org/10.1126/science.1194975

Damodaran, S., Parkin, K. L., & Fennema, O. R. (2007). *Food Science and Technology*. Florida:Boca Ratón, (Chapter 1).

Deroco, P. B., Medeiros, R. A., Rocha-filho, R. C., & Fatibello-filho, O. (2018). Selective and simultaneous determination of indigo carmine and allura red in candy samples at the nano-concentration range by fl ow injection analysis with multiple pulse amperometric detection. *Food Chemistry*, *247*(November 2017), 66–72. https://doi.org/10.1016/j.foodchem.2017.12.006

Guo, X., Wang, Y., Wu, F., Ni, Y., & Kokot, S. (2015). The use of tungsten disulfide dots as highly selective, fluorescent probes for analysis of nitrofurazone. *Talanta*, *144*, 1036–1043. https://doi.org/10.1016/j.talanta.2015.07.055

Ha, H. D., Han, D. J., Choi, J. S., Park, M., & Seo, T. S. (2014). Dual Role of Blue Luminescent MoS_2 Quantum Dots in Fluorescence Resonance Energy Transfer Phenomenon. *Small*, *10*(19), 3858–3862. https://doi.org/10.1002/smll.201400988

Huang, X., Zeng, Z., & Zhang, H. (2013). Metal dichalcogenide nanosheets: preparation, properties and applications. *Chemical Society Reviews*, *42*(5), 1934–1946. https://doi.org/10.1039/c2cs35387c

Ivani de Andrade, F., Florindo Guedes, M. I., Pinto Vieira, Í. G., PereiraMendes, N. F., Salmito Rodrigues, P. A., Costa Maia, C. S., Marqués Ávila, M. M., de Matos Ribeiro, L. (2014). Determination of synthetic food dyes in commercial soft drinks by TLC and ion-pair HPLC. *Food Chemistry*, *157*, 193–198. https://doi.org/10.1016/j.foodchem.2014.01.100

Lakowicz, J. R. (2006). *Principles of Fluorescence Spectroscopy* .New York, (Chapter 8)

Lesnyak, V., Gaponik, N., & Eychmu, A. (2013). Colloidal semiconductor nanocrystals: the aqueous approach. *Chemical Society Reviews*, *42*, 2905–2929. https://doi.org/10.1039/c2cs35285k

Li, B. L., Wang, J., Zou, H. L., Garaj, S., Lim, C. T., Xie, J., Li, N. B., Leong, D. T. (2016). Low-Dimensional Transition Metal Dichalcogenide Nanostructures Based Sensors. *Advanced Functional Materials*, *26*(39), 7034–7056. https://doi.org/10.1002/adfm.201602136

Liu, Q., Hu, C., & Wang, X. (2016). A facile one-step method to produce MoS_2 quantum dots as promising bio-imaging materials. *RSC Advances*, *6*(30), 25605–

25610. https://doi.org/10.1039/c6ra00572a

Liu, X., Zhang, W., Huang, L., Hu, N., Liu, W., Liu, Y., Li, S., Yang, C., Suo, Y., Wang, J. (2018). Fluorometric determination of dopamine by using molybdenum disulfide quantum dots. *Microchimica Acta*, *185*(4). https://doi.org/10.1007/s00604-018-2771-0

Magerusan, L., Pogacean, F., Coros, M., Socaci, C., Pruneanu, S., Leostean, C., & Pana, I. O. (2018). Green methodology for the preparation of chitosan / graphene nanomaterial through electrochemical exfoliation and its applicability in Sunset Yellow detection. *Electrochimica Acta*, *283*, 578–589. https://doi.org/10.1016/j.electacta.2018.06.203

Mazdeh, F. Z., Moradi, Z., Moghaddam, G., Moradi-Khatoonabadi, Z., Aftabdari, F. E., Badaei, P., & Hajimahmoodi, M. (2016). Determination of synthetic food colors, caffeine, sodium benzoate and potassium sorbate in sports drinks. *Tropical Journal of Pharmaceutical Research*, *15*(1), 183–188. https://doi.org/10.4314/tjpr.v15i1.25

Rodriguez, J. A., Ibarra, I. S., Miranda, J. M., Barrado, E., & Santos, E. M. (2016). Magnetic solid phase extraction based on fullerene and activated carbon adsorbents for determination of azo dyes in water samples by capillary electrophoresis. *Analytical Methods*, *8*(48), 8466–8473. https://doi.org/10.1039/c6ay02631a

Shen, Y., Zhang, X., Prinyawiwatkul, W., & Xu, Z. (2014). Simultaneous determination of red and yellow artificial food colourants and carotenoid pigments in food products. *Food Chemistry*, *157*, 553–558. https://doi.org/10.1016/j.foodchem.2014.02.039

Silva, M. L. S., Garcia, M. B. Q., Lima, J. L. F. C., & Barrado, E. (2007). Voltammetric determination of food colorants using a polyallylamine modified tubular electrode in a multicommutated flow system. *Talanta*, *72*(1), 282–288.

https://doi.org/10.1016/j.talanta.2006.10.032

Sinha, A., Dhanjai, Tan, B., Huang, Y., Zhao, H., Dang, X., Chen, J., Jain, R. (2018). MoS_2 nanostructures for electrochemical sensing of multidisciplinary targets: A review. *TrAC - Trends in Analytical Chemistry*, *102*, 75–90. https://doi.org/10.1016/j.trac.2018.01.008

Štengl, V., & Henych, J. (2013). Strongly luminescent monolayered MoS_2 prepared by effective ultrasound exfoliation. *Nanoscale*, *5*, 3387–3394. https://doi.org/10.1039/c3nr00192j

Sun, J., Li, X., Guo, W., Zhao, M., Fan, X., Dong, Y., Xu, C., Deng, J., Fu, Y. (2017). Synthesis Methods of Two-Dimensional MoS_2: A Brief Review. *Crystals*, *7*(7), 198. https://doi.org/10.3390/cryst7070198

Tang, Y., Sun, Z., Shen, J., Yu, J., Wang, S., Hao, J., Wang, B., Huang, Y., Liu, X., Zhuang, H. (2018). Peptide modified gold nanoclusters as a novel fluorescence detector based on quenching system of detecting Allura red. *Analytical Methods*, *10*, 5672–5678. https://doi.org/10.1039/c8ay01494a

Trojanowicz, M., & Kołacińska, K. (2016). Recent advances in flow injection analysis. *The Analyst*, *141*(7), 2085–2139. https://doi.org/10.1039/C5AN02522B

Union, C. of the E. (1994). European Parliament and Council Directive 94/35/EC of 30 June 1994 of sweeteners for use in foodstuffs. https://op.europa.eu/en/publication-detail/-/publication/576c6110-0270-429a-b445-8bdb40025cb4/language-en.

Vidal, M., Garcia-Arrona, R., Bordagaray, A., Ostra, M., & Albizu, G. (2018). Simultaneous determination of color additives tartrazine and allura red in food products by digital image analysis. *Talanta*, *184*(December 2017), 58–64. https://doi.org/10.1016/j.talanta.2018.02.111

Vilian, A. T. E., Dinesh, B., Kang, S. M., Krishnan, U. M., Huh, Y. S., & Han, Y. K.

(2019). Recent advances in molybdenum disulfide-based electrode materials for electroanalytical applications. *Microchimica Acta*, *186*, 203. https://doi.org/10.1007/s00604-019-3287-y

Wang, Yichao, Ou, J. Z., Balendhran, S., Chrimes, A. F., Mortazavi, M., Yao, D. D., Field, M. R., Latham, K., Bansal, V., Friend, J.R., Zhuiykov, S., Medhekar, N. V., Strano, M. S., Kalantar-Zadeh, K. (2013). Electrochemical control of photoluminescence in two-dimensional MoS_2 nanoflakes. *ACS Nano*, *7*(11), 10083–10093. https://doi.org/10.1021/nn4041987

Wang, Yong, & Ni, Y. (2014). Molybdenum disulfide quantum dots as a photoluminescence sensing platform for 2,4,6-trinitrophenol detection. *Analytical Chemistry*, *86*(15), 7463–7470. https://doi.org/10.1021/ac5012014

Wang, Z., & Dai, Z. (2015). Carbon nanomaterial-based electrochemical biosensors: An overview. *Nanoscale*, *7*(15), 6420–6431. https://doi.org/10.1039/c5nr00585j

Wilcoxon, J. P., Newcomer, P. P., & Samara, G. A. (1997). Synthesis and optical properties of MoS2 and isomorphous nanoclusters in the quantum confinement regime. *Journal of Applied Physics*, *81*(12), 7934–7944. https://doi.org/10.1063/1.365367

Xu, H., Yang, X., Li, G., Zhao, C., & Liao, X. (2015). Green Synthesis of Fluorescent Carbon Dots for Selective Detection of Tartrazine in Food Samples. *Journal of Agricultural and Food Chemistry*, *63*(30), 6707–6714. https://doi.org/10.1021/acs.jafc.5b02319

Xu, S., Li, D., & Wu, P. (2015a). One-pot, facile, and versatile synthesis of monolayer MoS2 /WS2 quantum dots as bioimaging probes and efficient electrocatalysts for hydrogen evolution reaction. *Advanced Functional Materials*, *25*(7), 1127–1136. https://doi.org/10.1002/adfm.201403863

583 Yu, Y., & Fan, Z. (2016). Magnetic solid-phase extraction coupled with HPLC for the
584 determination of Allura Red in food and beverage samples. *Food Additives and*
585 *Contaminants - Part A*, *33*(10), 1527–1534.
586 https://doi.org/10.1080/19440049.2016.1231937
587 Zhang, W., Wang, Y., Zhang, D., Yu, S., Zhu, W., Wang, J., … Wang, J. (2015). A
588 one-step approach to the large-scale synthesis of functionalized MoS_2 nanosheets
589 by ionic liquid assisted grinding. *Nanoscale*, *7*(22), 10210–10217.
590 https://doi.org/10.1039/c5nr02253c
591 Zhang, X., Lai, Z., Liu, Z., Tan, C., Huang, Y., & Li, B. (2015). A Facile and Universal
592 Top-Down Method for Preparation of Monodisperse Transition-Metal
593 Dichalcogenide Nanodots. *Angewandte Chemie*, *54*, 5425–5428.
594 https://doi.org/10.1002/anie.201501071
595 Zhao, M., Chen, A.-Y., Huang, D., Chai, Y.-Q., Zhuo, Y., & Yuan, R. (2017). MoS_2
596 Quantum Dots as New Electrochemiluminescence Emitters for Ultrasensitive
597 Bioanalysis of Lipopolysaccharide. *Analytical Chemistry*, *89*(16), 8335–8342.
598 https://doi.org/10.1021/acs.analchem.7b01558
599
600

Figure Captions

Figure 1. (A) HR-TEM image of the MoS_2-dots with 10 nm scale. The inset shows a selected area electron diffraction (SAED) pattern. (B) Higher magnification showing the lattice fringes of a MoS_2-dots. (C) A line profile indicating the d-spacing in the selected MoS_2-dots.

Figure 2. (A) Absorption spectra of AR (a) and fluorescence spectra of MoS_2-dots at different λ_{exc} (dotted lines). (B) Fluorescence spectra of MoS_2-dots in absence (a) and in presence of 2.0×10^{-5} M AR (b). λ_{exc} = 370 nm. MoS_2-dots diluted 1:100 in H_3PO_4/NaH_2PO_4 0.1M pH 2.

Figure 3. Fluorescence inhibition at 475 nm for increasing AR concentrations at different temperatures. The legend includes the Ksv values calculated from the slopes of the corresponding experiments.

Figure 4. A) FIAgrams of MoS_2-dots and MoS_2-dots with increasing concentrations of AR. B) Calibration plot of $\%If_0$ with increasing concentration of AR. L= 40 cm; Di = 0.5 mm; Q = 3 mL/min; V_{inj} = 100 µL. MoS_2-dots 1:150 in H_3PO_4/NaH_2PO_4 0.1M pH 2. λ_{exc} = 370 nm; λ_{em} = 475 nm.

Figure 5. FIAgrams of MoS_2-dots and MoS_2-dots with non-spiked and spiked samples L= 40 cm; Di = 0.5 mm; Q = 3 mL/min; V_{inj} = 100 µL. MoS_2-dots 1:150 in H_3PO_4/NaH_2PO_4 0.1M pH 2. λ_{exc} = 370 nm; λ_{em} = 475 nm.

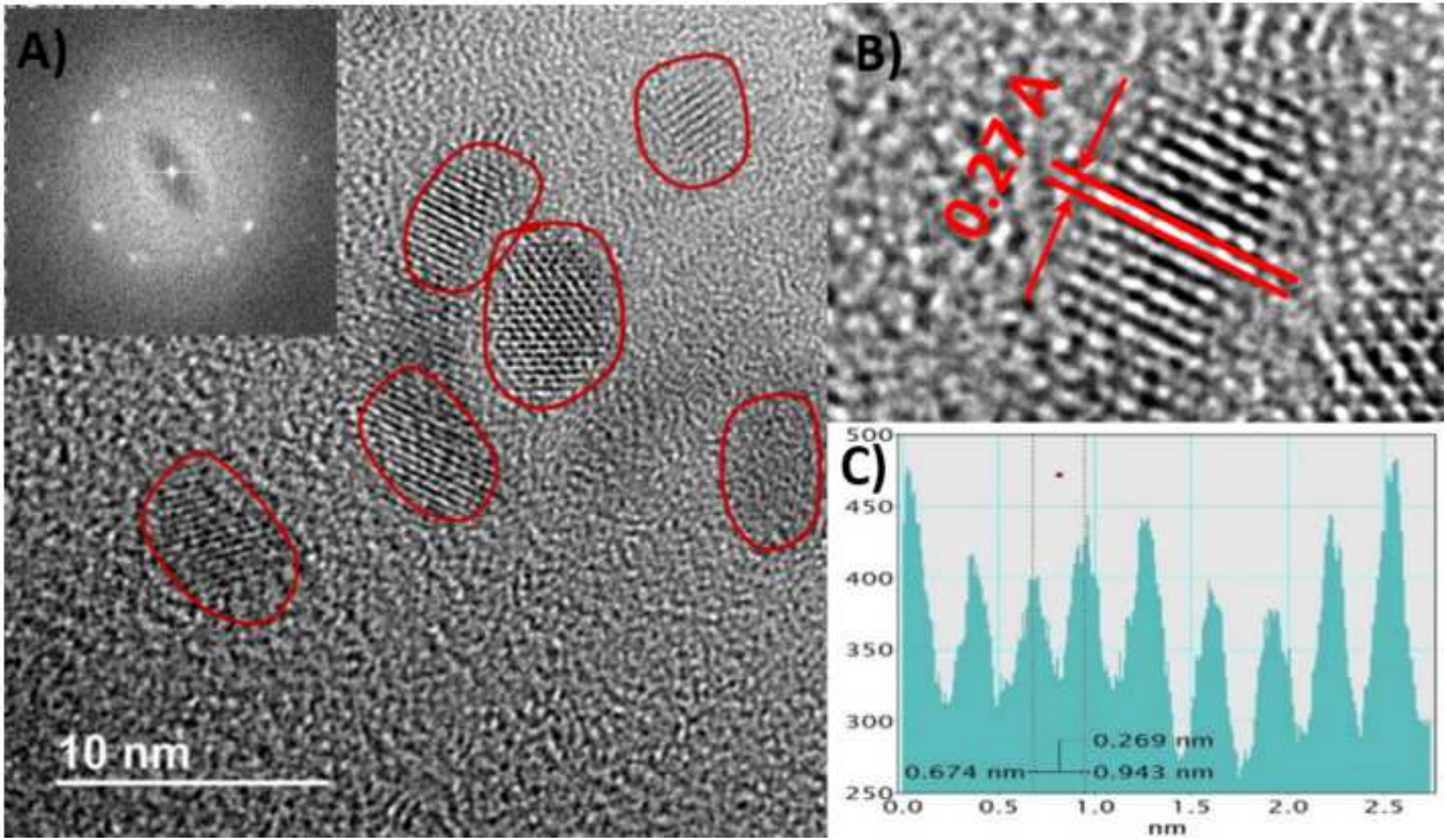
A)
10 nm
B)
0.27 A
C)
500
450
400
350
300
250
0.269 nm
0.674 nm
0.943 nm
0.0
0.5
1.0
1.5
2.0
2.5
nm

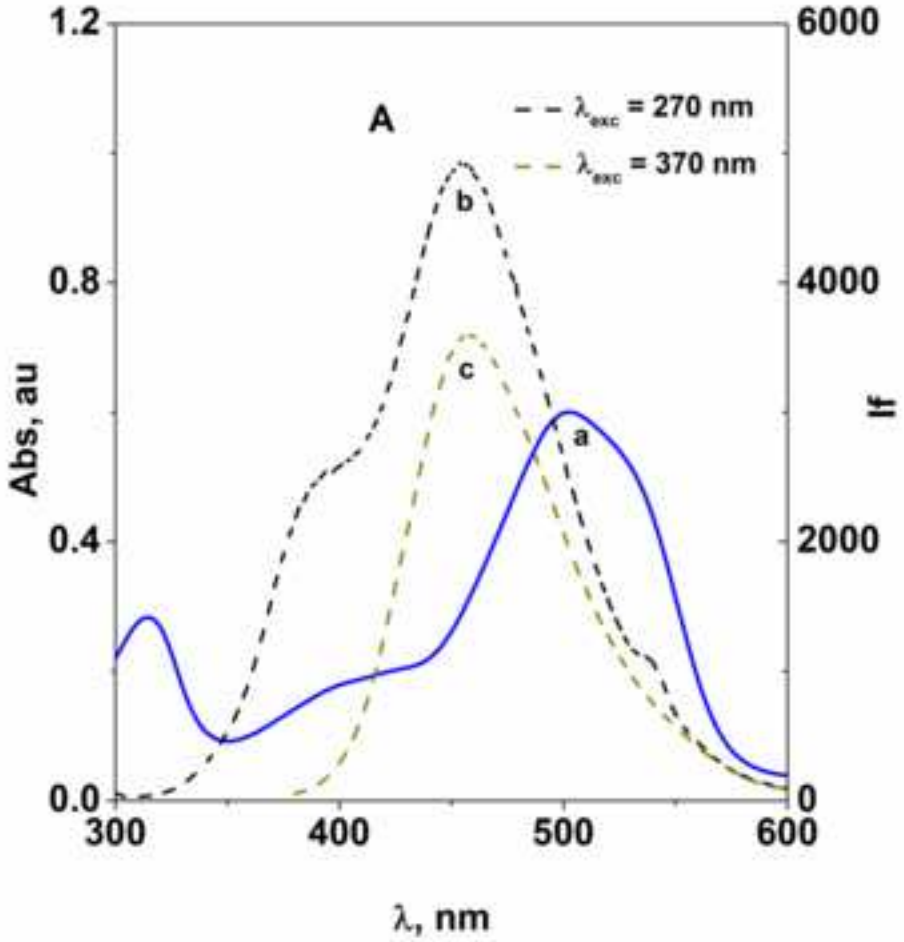
A
λ_{exc} = 270 nm
λ_{exc} = 370 nm
a
b
c
Abs, au
If
λ, nm
1.2
0.8
0.4
0.0
6000
4000
2000
0
300
400
500
600

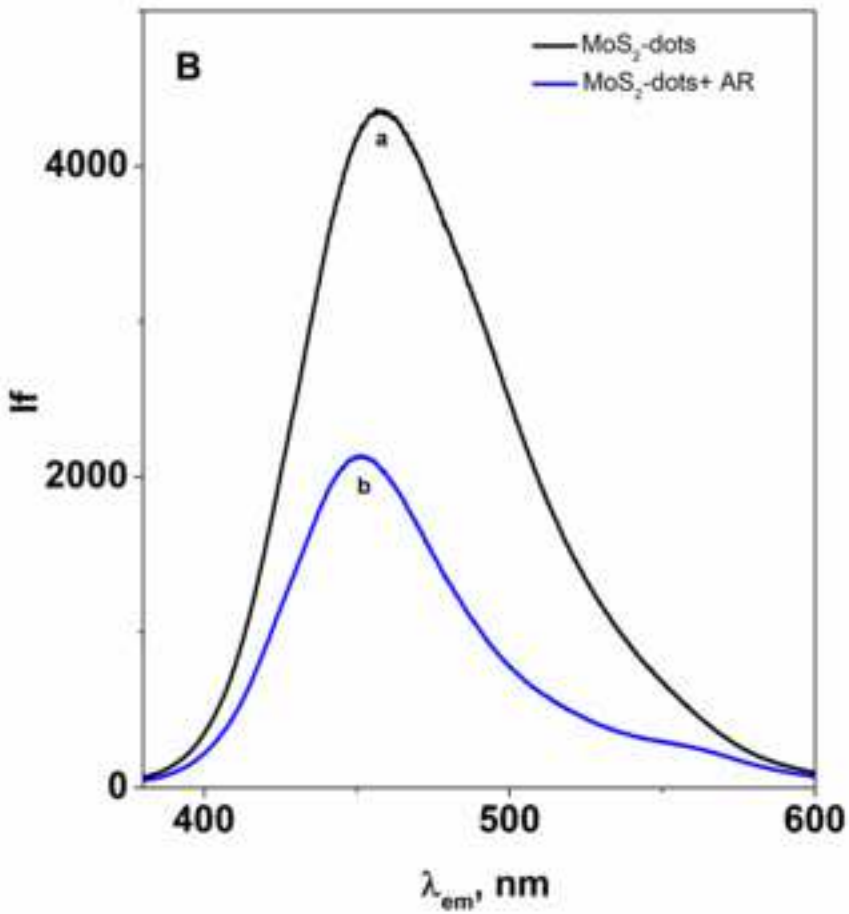
B
MoS_2-dots
MoS_2-dots+ AR
a
b
If
λ_{em}, nm
4000
2000
0
400
500
600

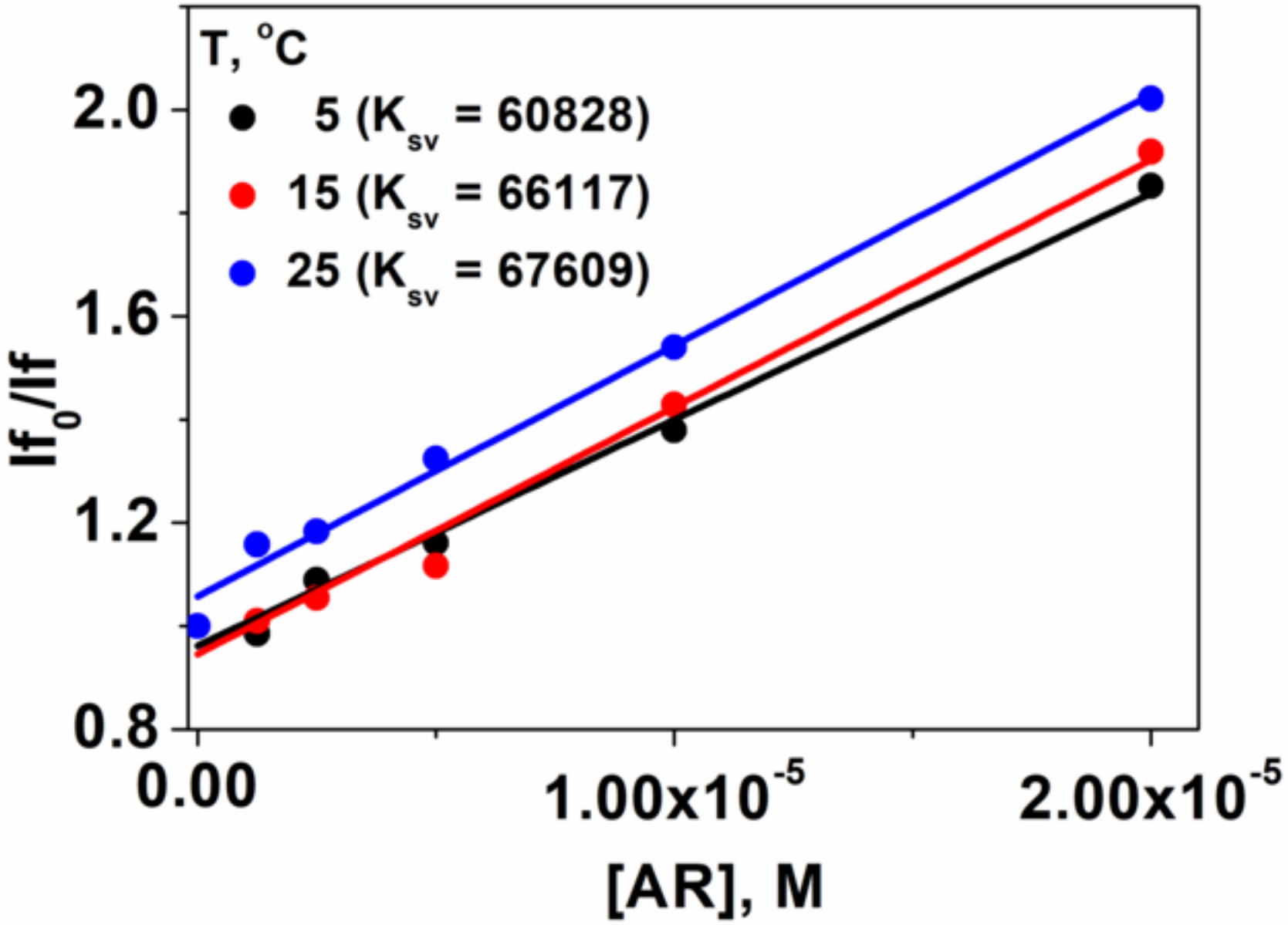
T, °C
5 (K_sv = 60828)
15 (K_sv = 66117)
25 (K_sv = 67609)
If_0/If
2.0
1.6
1.2
0.8
0.00
1.00x10^-5
2.00x10^-5
[AR], M

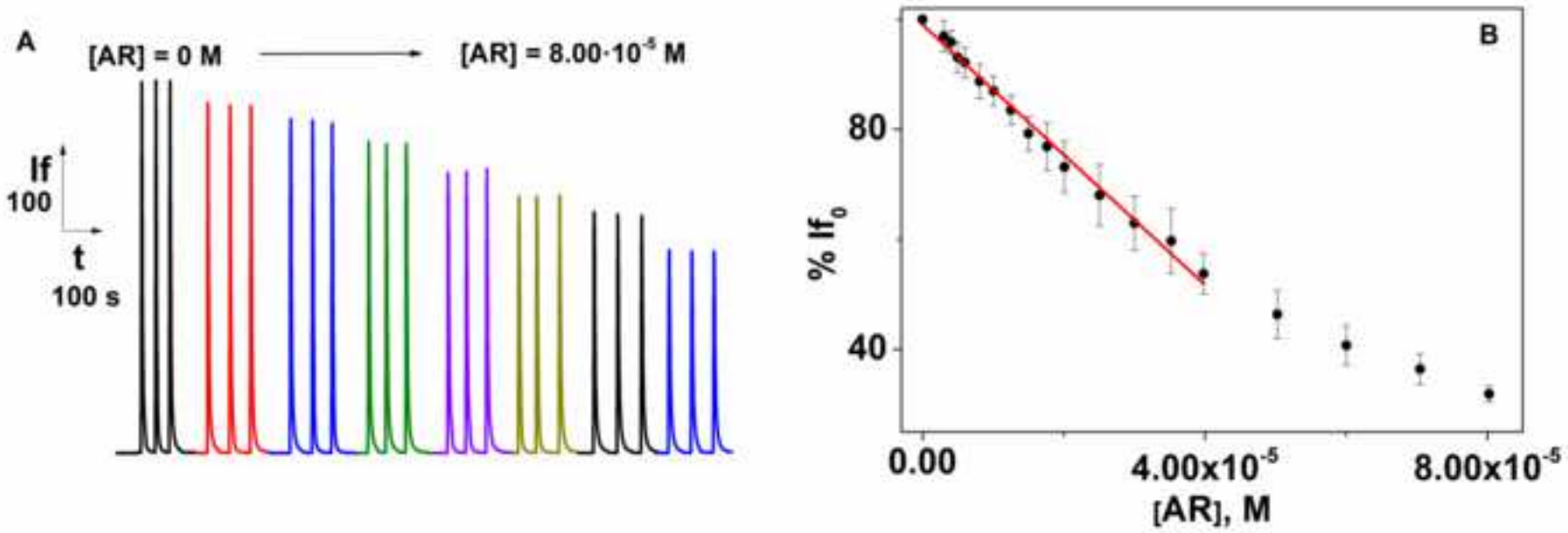
A
[AR] = 0 M
[AR] = 8.00·10⁻⁵ M
If
100
t
100 s
B
80
40
% If0
0.00
4.00x10-5
8.00x10-5
[AR], M

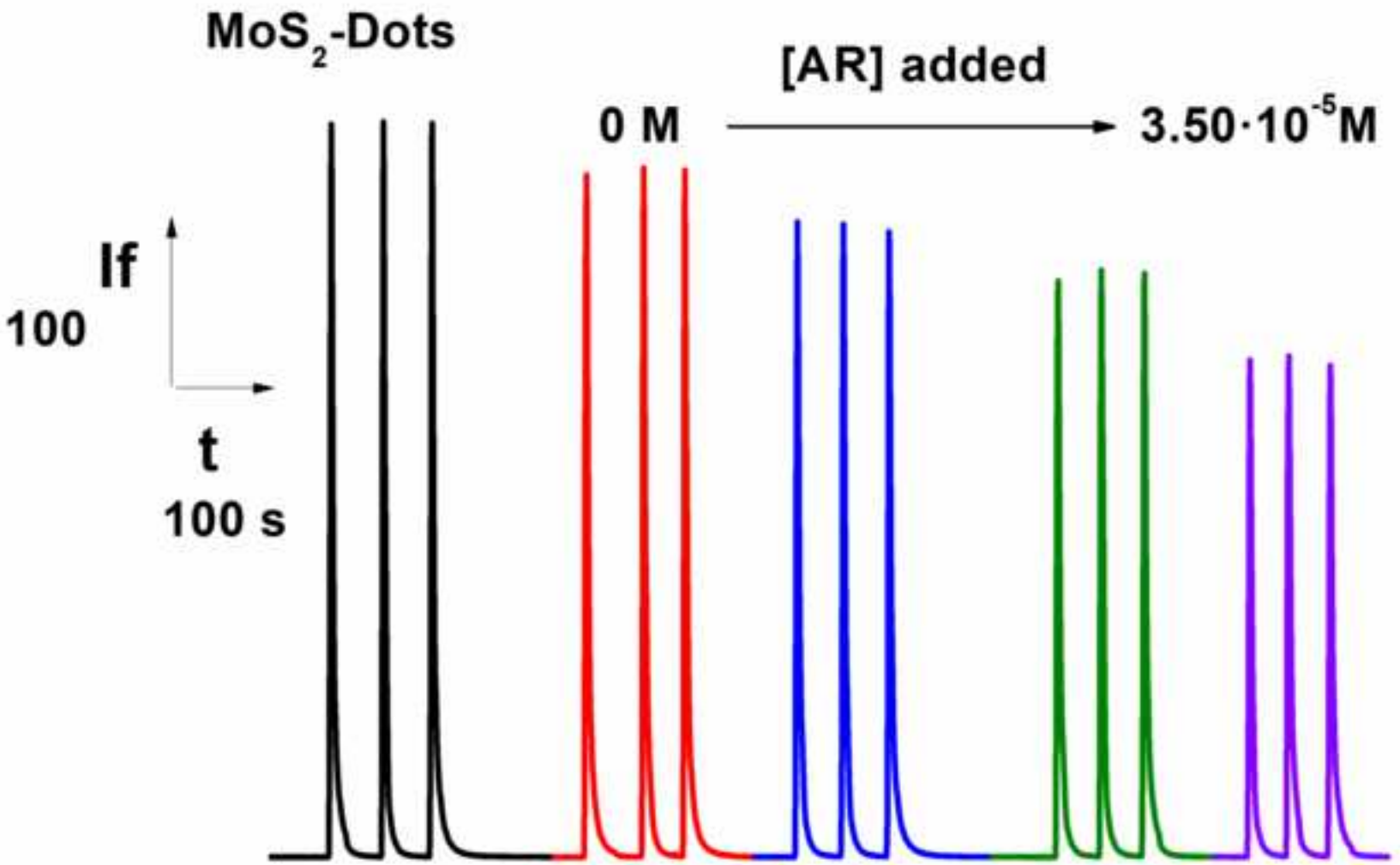
MoS2-Dots
[AR] added
0 M
3.50·10-5M
If
100
t
100 s

Supplementary Material

MoS_2 quantum dots for on-line fluorescence determination of the food additive allura red in beverage.

Alicia Coloma[a], María del Pozo[a]*, Rut Martínez-Moro[a], Elias Blanco[a], Pedro Atienzar[b], Lorenzo Sánchez[c], María Dolores Petit-Domínguez[a], Elena Casero[a], Carmen Quintana[a]

[a]*Departamento de Química Analítica y Análisis Instrumental, Universidad Autónoma de Madrid, Cantoblanco, 28049 Madrid, Spain.*

[b]*Instituto Universitario de Tecnología Química CSIC-UPV, Departamento de Química, Universidad Politécnica de Valencia, 46022 Valencia, Spain.*

[c] *Departamento de Medio Ambiente. Geología Ambiental Aplicada. CIEMAT. Avda. Complutense, 40 Edif. 85, 28040 Madrid. Spain*

*maria.delpozo@uam.es; Phone: +34 914975619; Fax: +34914974931

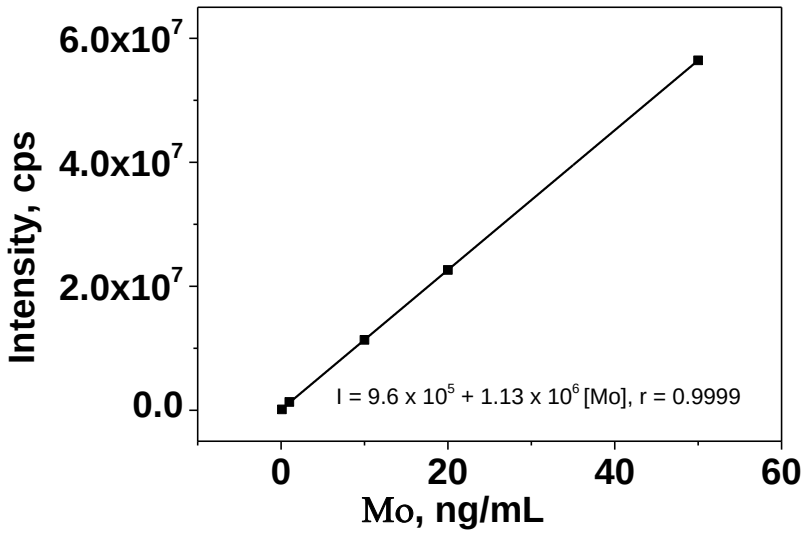

Figure S1. ICP-MS calibration graphs corresponding to Mo determination in the synthetized suspensions

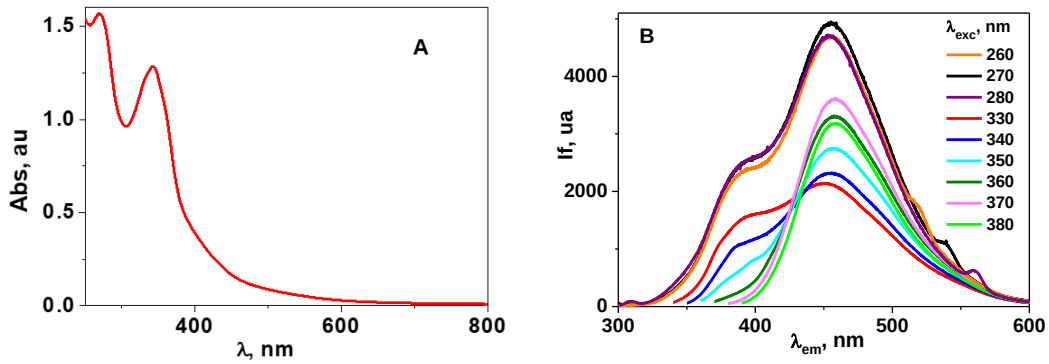

Figure S2. A: UV-VIS absorption spectrum of MoS_2-dots 1:100 diluted in water. B: MoS_2-dots fluorescence spectra recorded at λ_{exc} between 260-380 nm.

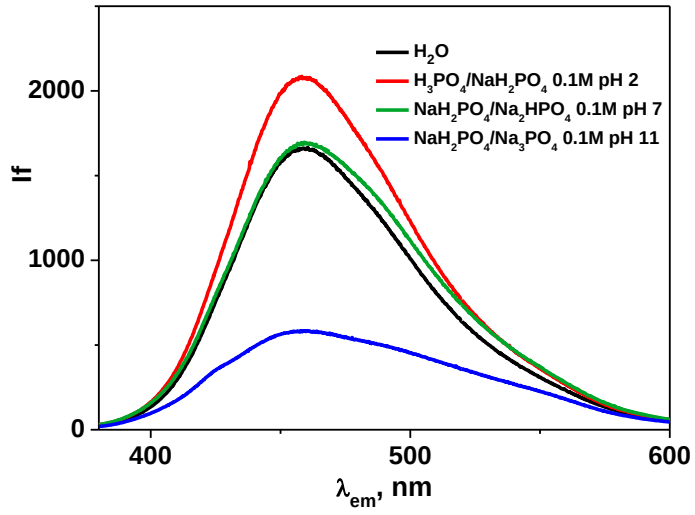

Figure S3. MoS_2-dots spectra recorded for 1:100 dilution at different pH values. λ_{exc} = 370 nm.

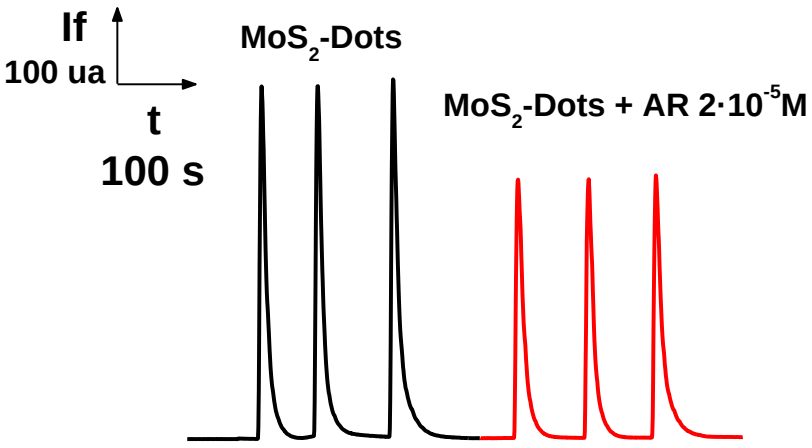

Figure S4. FIA-graphs of MoS_2-dots and MoS_2-dots-AR. [AR] = 2.0×10^{-5} M; H_3PO_4/NaH_2PO_4 0.1 M pH2; MoS_2-dots diluted 1:150 in H_3PO_4/NaH_2PO_4 0.1 M pH 2. Reactor length (L) = 40 cm; Reactor internal diameter (Di) = 0.5 cm; Injection volume (V_{inj}) = 100 µL; Caudal (Q) = 1 mL/min; λ_{exc} = 370 nm; λ_{em} = 475 nm.

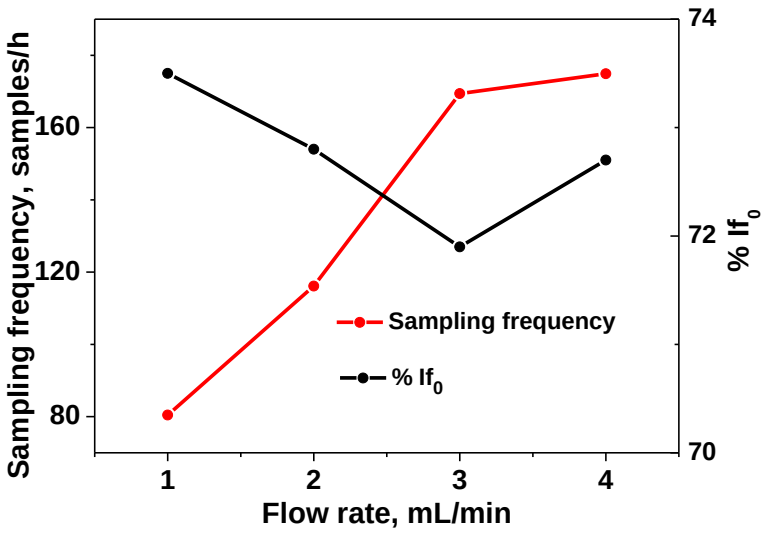

Figure S5. % If_0 and sampling frequency variation with the carrier flow rate. L = 40 cm; Di = 0.5 cm; V_{iny} = 100 µL. MoS_2-dots 1:150 in H_3PO_4/NaH_2PO_4 0.1M pH 2. [AR] = $2.00 \cdot 10^{-5}$ M, λ_{exc} = 370 nm; λ_{em} = 475 nm.

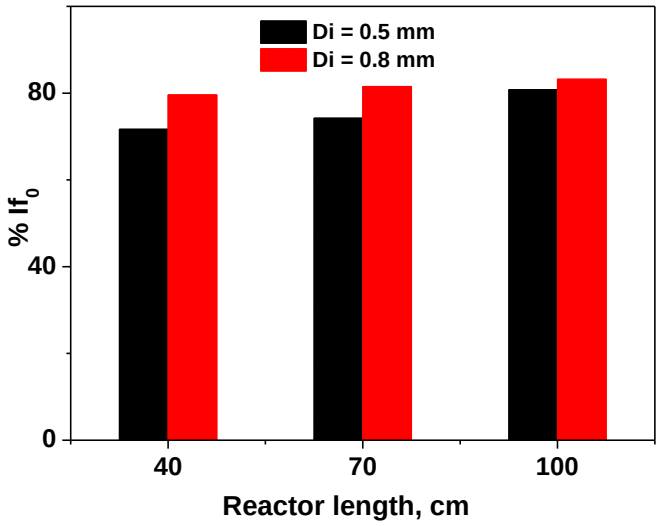

Figure S6. Influence of both, length and internal diameter of the reactor, in the % If_0. V_{iny} = 100 µL; Q = 3 mL/min. MoS_2-dots 1:150 in 0.1M H_3PO_4/NaH_2PO_4 pH 2. [AR] = $2.00 \cdot 10^{-5}$ M, λ_{exc} = 370 nm; λ_{em} = 475 nm.

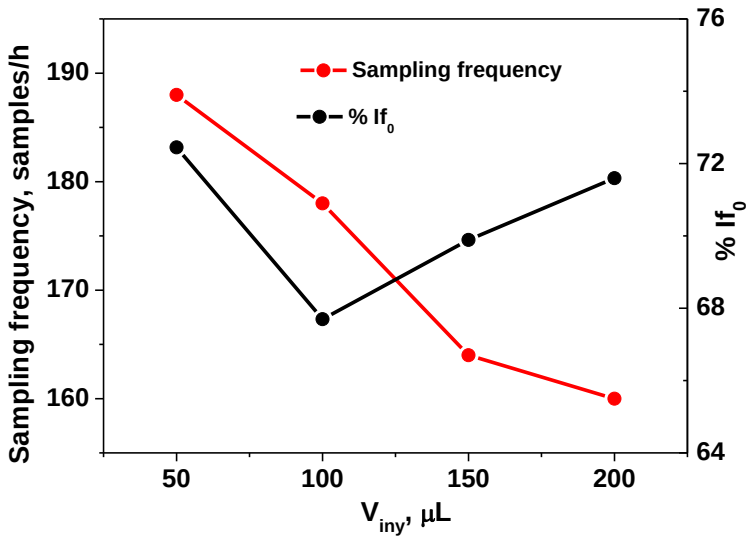

Figure S7. Variation of both, % If_0 and sampling frequency, with the injection volume. L= 40 cm; Di = 0.5 mm; Q = 3 mL/min. MoS_2-dots 1:150 in H_3PO_4/NaH_2PO_4 0.1M pH 2. [AR] = $2.00 \cdot 10^{-5}$ M, λ_{exc} = 370 nm; λ_{em} = 475 nm.

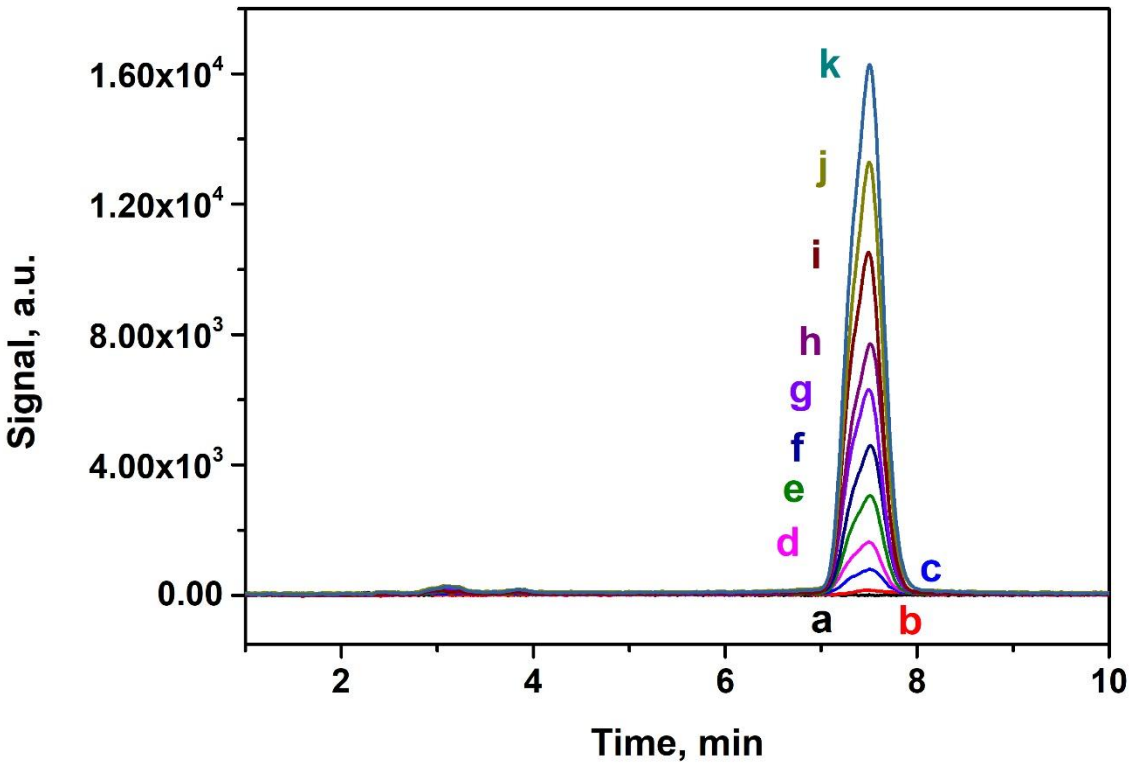

Figure S8. Chromatograms corresponding to solutions containing increasing concentrations of AR recorded at the HPLC-UV-Vis system (a) Mobile phase, (b) 2.0 10^{-7}, (c) 1.1 10^{-6},(d) 2.1 10^{-6},(e) 4.0 10^{-6}, (f) 6.0 10^{-6}, (g) 8.1 10^{-6}, (h) 1.0 10^{-5}, (i) 1.3 10^{-5} M, (j) 1.6 10^{-5} M and (k) 2.0 10^{-5} M.

Table S1. Hydrodynamic and geometrical parameter optimization.

Parameter	Range assays	Optimal value
[MoS_2-Dots] (dilution 1:X)	50-200	150
Flow rate (Q) (mL/min)	1-4	3
Reactor length (L) (cm)	40-100	40
Reactor internal diameter (Di) (mm)	0.5-0.8	0.5
Injection volume (V_{inj}) (μL)	50-200	100

Table S2. Comparative methods for AR determination

Method	LOD (mol/L)	Linear Range (mol/L)	Reference
Digital image analysis	1.29×10^{-6}	4.29×10^{-6} – 5.57×10^{-5}	(Vidal, Garcia-Arrona, Bordagaray, Ostra, & Albizu, 2018)
Amperometric-FIA (polyallylamine - GCTE)	1.40×10^{-6}	1.00×10^{-5} – 1.50×10^{-4}	(Silva, Garcia, Lima, & Barrado, 2007)
MPA-FIA (BDD/p-silicon)	7.00×10^{-9}	4.00×10^{-8} – 7.70×10^{-7}	(Deroco, Medeiros, Rocha-filho, & Fatibello-filho, 2018)
MSPE-CE	4.29×10^{-6}	1.29×10^{-5} – 8.58×10^{-5}	(Rodriguez, Ibarra, Miranda, Barrado, & Santos, 2016)
AuNCs-Peptide Fluorescence	6.67×10^{-7}	2.00×10^{-6} – 9.00×10^{-5}	(Tang et al., 2018)
UPLC-MS	2.57×10^{-8}	1.00×10^{-7} – 2.79×10^{-6}	(Al Shamari et al., 2020)
HPLC-UV	1.09×10^{-6}	-	(Mazdeh et al., 2016)
MoS_2-dots FIA-fluorescence	1.70×10^{-6}	5.00×10^{-6} – 4.00×10^{-5}	This work

GCTE: Glassy carbon tubular electrode; MPA-FIA: Multiple pulse amperometric Flow injection analysis. BDD/p-silicon: Boron-doped diamond/ p-silicon; MSPE-CE: Magnetic solid phase extraction coupled to capillary electrophoresis; AnNCs-Peptide: gold nanoclusters modified with peptide; UPLC-MS: Ultra performance liquid chromatography-mass spectrometry; HPLC-UV: High performance liquid chromatography couple to ultraviolet detector